Numerical Average-Value Model of Voltage-Source Converters with Overmodulation and Duty-Cycle Limit

Md Jobayead Hossan
School of Electrical Engineering and Computer Science
Washington State University
Pullman, USA
md.jobayeadhossan@wsu.edu

Seyyedmilad Ebrahimi
School of Electrical Engineering and Computer Science
Washington State University
Pullman, USA
s.ebrahimi@wsu.edu

Juri Jatskevich
Department of Electrical and Computer Engineering
The University of British Columbia
Vancouver, Canada
jurij@ece.ubc.ca

***Abstract*—Average-value models (AVMs) of voltage-source converters (VSCs) are indispensable for efficient computer simulations when lower-frequency dynamics are of particular interest in the studies rather than the switching phenomena. The conventional AVMs of VSCs primarily assume operation in the linear region, where the ac output voltages increase linearly with an increase in the converter modulation index. However, VSCs may also operate in the overmodulation region where the modulation index is increased beyond unity, e.g., in motor drive applications to increase the dc-link voltage utilization. Under overmodulation, VSCs exhibit nonlinear output characteristics. Additionally, in practice, the duty-cycle for the VSC switching operation is typically limited to below 100%, which is often ignored in the conventional AVMs despite its impact on dynamic performance. In this paper, a new AVM is proposed for VSCs that is capable of capturing both the linear and nonlinear characteristics of VSCs, while incorporating the effects of duty-cycle limit and third-harmonic injection. The superior accuracy of the proposed AVM against the conventional AVMs of VSCs is demonstrated through dynamic simulations of a variable-frequency motor drive system.**

***Index Terms*--Average-value model (AVM), duty-cycle limit, overmodulation, third harmonic injection, voltage source converter (VSC).**

I. INTRODUCTION

Dc–ac voltage-source converters (VSCs) have become an indispensable technology in modern electric power systems, e.g., as the interface for integration of renewable resources, ac motor drives, etc. Various studies of such systems, such as dynamic performance evaluation, controller design/tuning, and stability analysis, require electromagnetic transient (EMT) simulations. The validity of EMT simulations for these systems heavily relies on accurate models of VSCs [1].

Detailed switching models of VSCs can accurately capture the high-frequency discrete operation of individual converter switches. However, they introduce a significant computational burden for system-level studies where only the lower-frequency dynamic behaviour of the whole converter is desired [2].

To address this, average-value models (AVMs) have been developed for VSCs [1]–[5]. AVMs enable significantly faster simulations compared to the switching models, albeit at the expense of ignoring high-frequency switching ripples.

Although the dc–ac VSCs often operate in their linear modulation region, where the converter's output ac voltages change linearly with the modulation index [6], in practice, VSCs may also operate in their overmodulation region to maximize the dc voltage utilization under demanding conditions [7], e.g., during motor acceleration. The output characteristic in the overmodulation region is nonlinear, where increasing the converter's modulation index will result in less increase in the ac output voltage [6].

The so-called third-harmonic injection technique increases the linear region of the output characteristic by modifying the three-phase modulating signals to include third-harmonic components. This increases the dc voltage utilization by ~15% [7] without entering the overmodulation region. Nevertheless, operating in the overmodulation region may be inevitable, either due to limited available dc voltage or for achieving other control objectives [7]–[11].

The analytical methods to consider the nonlinearities in the overmodulation region often involve detailed Fourier analysis to characterize the voltage gain and are complicated [11], [12]. Additionally, in practice, the switches in PWM-controlled VSCs are operated with a duty-cycle limit below 100% [13] for safety considerations. This also alters the output characteristics of the converter, making the analytical modeling challenging [14] when considered in conjunction with overmodulation. Consequently, most of the existing AVMs of VSCs assume that the converter operates in its linear region [1]–[5], and ignore the nonlinearities introduced by the overmodulation.

This paper investigates how the nonlinearities in the overmodulation region impact modeling of an ac motor variable frequency drive (VFD) system. A new numerical AVM is also developed for VSCs, that is capable of capturing the nonlinear characteristics of the overmodulation and duty-cycle limits, with and without third-harmonic injections. The accuracy of the proposed AVM is then verified against the detailed switching model as well as the conventional AVM counterparts.

979-8-3315-8138-1

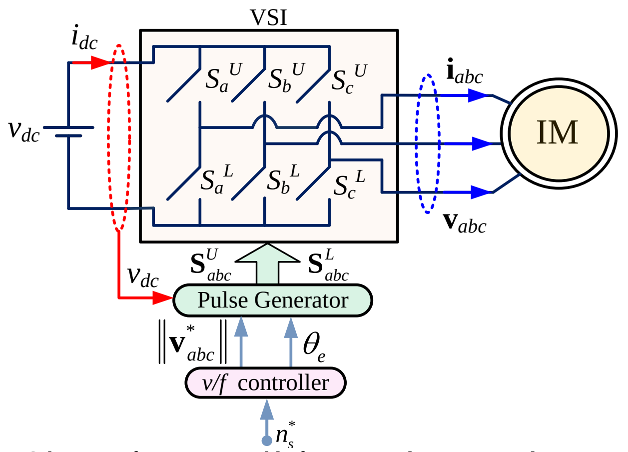

Fig. 1. Schematic of a generic variable-frequency induction motor drive system with a voltage source inverter using a volts-per-hertz control scheme.

II. Motor Drive System

The motor drive system depicted in Fig. 1 is considered in this paper to represent a typical VFD configuration. Specifically, the VFD includes a voltage-source inverter (VSI) that provides variable-frequency ac voltages to the stator of an induction motor (IM) to regulate the rotor speed. It is assumed that the dc-link is supplied from a dc source with voltage v_{dc}.

A. VFD Controller

Here, for regulating the motor speed, an open-loop volts-per-hertz (*v/f*) controller is considered in Fig. 1. The controller receives the speed command n_s^* (i.e., synchronous speed in rpm) and computes the angle of the stator voltages as

$$\theta_e = \int \omega_e^* dt , \qquad (1)$$

where ω_e^* is the reference angular speed (in rad/s) calculated as

$$\omega_e^* = 2\pi f_e^* = \left(\frac{\pi}{60}\right) \times P \times n_s^* . \qquad (2)$$

In (2), f_e^* is the reference frequency of the stator voltages in Hz, and P is the number of poles of the motor. The *v/f* controller also computes the required magnitude of (the fundamental frequency components of) the ac voltages as

$$\left\| \mathbf{v}_{abc}^* \right\| = \Gamma_{v/f} \times f_e^* , \qquad (3)$$

where $\Gamma_{v/f}$ is the controller's *v/f* ratio. It is noted that a slew-rate block may also be used to limit the rate of change of the speed command for a smooth operation [15].

B. Pulse Generation

The pulse generation block in Fig. 1 receives the magnitude and angle of the reference ac voltages (i.e., $\left\| \mathbf{v}_{abc}^* \right\|$ and θ_e), and computes the required signals for the operation of the six VSI switches, i.e., $\mathbf{S}_{abc}^U$ for the three upper switches, and $\mathbf{S}_{abc}^L$ for the three lower switches. It is assumed that the two switches in each leg/phase operate in a complementary manner [6] based on a sinusoidal pulse width modulation (SPWM) switching scheme.

1) SPWM with sinusoidal references: In the conventional SPWM technique, a high-frequency carrier signal v_{crr} [i.e., the triangular wave (I) in Fig. 2(a) whose frequency is down-scaled for better visibility] is compared to three ±120° shifted sinusoidal reference signals that are generated for each phase as

$$\mathbf{m}_{abc} = \begin{bmatrix} m_a \\ m_b \\ m_c \end{bmatrix} = M \times \begin{bmatrix} \cos(\theta_e) \\ \cos(\theta_e - 2\pi/3) \\ \cos(\theta_e + 2\pi/3) \end{bmatrix} . \qquad (4)$$

Here, M is the modulation index that relates the magnitude of the ac voltages to the dc voltage and is defined as

$$M = \frac{\left\| \mathbf{v}_{abc}^* \right\|}{v_{dc}/2} . \qquad (5)$$

If the modulation index is limited to $0 \le M \le 1$, the amplitude of the modulation signals m_j where $j \in \{a,b,c\}$ will be lower than the peak of the carrier signal, as shown in Fig. 2(a) with the blue curve (II). In this case, increasing M will result in a linear increase in the amplitude of the output ac voltages [6]. Whereas, if $M > 1$ the amplitude of m_j will be higher than the peak of the carrier signal (i.e., overmodulation), as shown in Fig. 2(a) with the red curve (III). In this case, increasing M will result in a smaller increase in the amplitude of the output ac voltages, i.e., the ability of the converter to raise the output voltage diminishes, and the characteristic becomes nonlinear [6]. The gate signals for the upper switch S_j^U of the associated phase j in the linear and nonlinear/overmodulation regions are depicted in Figs. 2(b) and 2(c), respectively.

As seen in Fig. 2(c), with overmodulation, the gate pulse saturates at 100% duty-cycle for a portion of the fundamental cycle. However, realistically, for practical considerations, the duty-cycle is typically limited to 95–98% [13]. This is achieved by considering a cap for the modulating signal (e.g., at ~96% of the carrier signal), as illustrated in Fig. 2(a) with the green curve (IV). The associated gate signal for the upper switch S_j^U is shown in Fig. 2(d) where the duty cycle is limited to ~96%. This duty-cycle limit affects the amplitude of the output ac voltages.

2) SPWM with 3rd harmonic injection: To extend the linear region of the characteristic, the modulating signals can be modified by injecting 3rd harmonic components as [11]

$$\mathbf{m}_{abc}^{3H} = \begin{bmatrix} m_a^{3H} \\ m_b^{3H} \\ m_c^{3H} \end{bmatrix} = M \times \left(\begin{bmatrix} \cos(\theta_e) \\ \cos(\theta_e - 2\pi/3) \\ \cos(\theta_e + 2\pi/3) \end{bmatrix} - \frac{1}{6} \begin{bmatrix} \cos(3\theta_e) \\ \cos(3\theta_e) \\ \cos(3\theta_e) \end{bmatrix} \right) . \qquad (6)$$

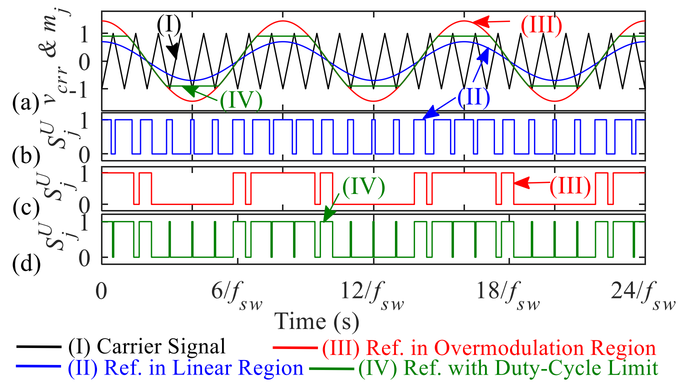

Fig. 2. Sinusoidal PWM scheme: (a) carrier and modulating signals under linear, overmodulation, and duty-cycle limit operation, (b) gate pulse in linear region, (c) gate pulse in nonlinear region, (d) gate pulse with duty-cycle limit.

979-8-3315-8138-1

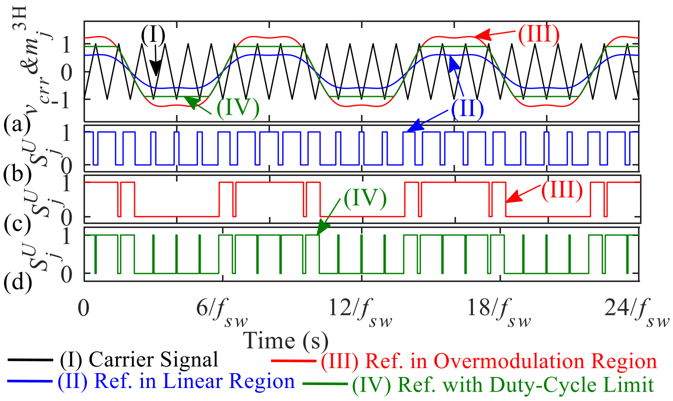

Fig. 3. Sinusoidal PWM with 3rd harmonic injection: (a) carrier and modulating signals under linear, overmodulation, and duty-cycle limit operation, (b)–(d) their corresponding gate pulses for the upper switch.

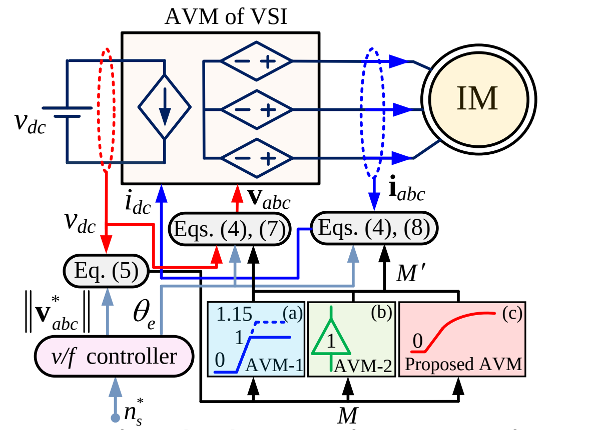

Fig. 4. Circuit interface and implementation of various AVMs of VSCs: (a) conventional AVM-1, (b) conventional AVM-2, (c) proposed AVM.

Injection of the 3rd harmonic components results in a flattened top for the modulating signal, as shown in Fig. 3(a). Given that the 3rd harmonics cancel out in the line voltages, this allows for scaling up M by a factor of $2/\sqrt{3}$ (i.e., ~15.5%) [7], [11] without exceeding the carrier's peak; therefore, enabling a higher dc bus utilization in the linear region. The modulating signals in the linear region, overmodulation region, and with duty-cycle limit are shown in Fig. 3(a) as curves (II)–(IV), respectively. The associated gate signals for the upper switch S_j^U are also shown in Figs. 3(b)–3(d), respectively.

III. Average-Value Modeling of VSCs

In AVMs, the high-frequency switching ripples are ignored, allowing the average dynamics to be captured. For circuit interfacing, the discrete switches are replaced with controlled voltage and current sources, as illustrated in Fig. 4. In AVMs, the relationship between the average values of the dc terminal variables of the VSC is related to the fundamental components of the ac terminal variables. Specifically, the (fundamental frequency) ac voltages are expressed based on (4), (5) as

$$\mathbf{v}_{abc} = \begin{bmatrix} v_a & v_b & v_c \end{bmatrix}^T = \begin{bmatrix} m_a & m_b & m_c \end{bmatrix}^T \times \frac{v_{dc}}{2}. \qquad (7)$$

The (average value) of the dc current can be calculated using the power balance ($P_{dc} = v_{dc} i_{dc} = v_a i_a + v_b i_b + v_c i_c = P_{ac}$) as

$$i_{dc} = \frac{1}{2} \times \left(m_a i_a + m_b i_b + m_c i_c \right). \qquad (8)$$

A. Conventional AVMs

The implementations of two instances of the conventional AVMs are shown in Figs. 4(a), 4(b). Therein, the dc voltage is measured and used along with the reference magnitude of the ac voltages from the *v/f* controller to compute the modulation index based on (5). In AVM-1, the modulation index is passed through a saturation block (either with an upper bound of 1 for standard SPWM or 1.15 for SPWM with 3rd harmonic injection) to operate in the linear region. In AVM-2, the modulation index, computed based on the output of the controller, is not bounded, allowing it to operate in the overmodulation region with $M > 1$. In both AVMs, the output M' is then used along with θ_e and measured v_{dc} to calculate the ac voltages based on (4), (7); and along with θ_e and measured $\mathbf{i}_{abc}$ to calculate the dc current based on (4), (8).

B. Proposed AVM

Both conventional AVM-1 and conventional AVM-2 are incapable of capturing the nonlinear characteristic of the VSCs when operated in the overmodulation region. Additionally, they lack a mechanism to account for the effect of the PWM duty-cycle limit on the output voltage. In this paper, a new AVM is proposed that captures both the linear and nonlinear characteristics of the VSCs, spanning all possible operating regions. This is achieved by using a numerical lookup table, as shown in Fig. 4 via model (c), which captures the nonlinear relation between the output voltage and modulation index in the overmodulation region. Specifically, the proposed numerical AVM can also incorporate the effect of the 3rd harmonic injection (in both linear and overmodulation regions) as well as the PWM duty-cycle limit on the output voltage characteristic through its embedded lookup table. As demonstrated in Fig. 4, the modulation index M computed based on the output of the controller is passed into the numerical lookup table, and the output M' is used to compute the output ac voltages and the dc current based on (4), (7), (8), similar to AVM-1 and AVM-2.

Establishing the lookup tables for the proposed AVM is straightforward. For this purpose, the detailed switching model is simulated according to the desired switching scheme, and the modulation index M is varied over the desired range (e.g., from 0 to 2.5 using a ramp function). Then, the fundamental frequency component of the output ac voltages is extracted, and the modified modulation index M' is calculated based on (5) and stored in a 1-D lookup table with respect to the original M. Because the VSC uses forced switching, the load at the ac terminal can be arbitrary, e.g., a simple *RL* branch.

The output characteristic of the VSC (i.e., magnitude of the fundamental frequency ac voltages $\|\mathbf{v}_{abc}^1\|$ per unit of $v_{dc}/2$) is shown in Fig. 5. Therein, the profiles obtained by the switching model with four switching schemes (i.e., Case-A: standard SPWM with sinusoidal modulating signals, Case-B: sinusoidal with 3rd harmonic injection, Case-C: sinusoidal with duty-cycle limit, and Case-D: sinusoidal with 3rd harmonic injection and duty-cycle limit) are depicted. The data from the proposed AVM under similar SPWM schemes are also superimposed, which are consistent with the switching model. The output

979-8-3315-8138-1

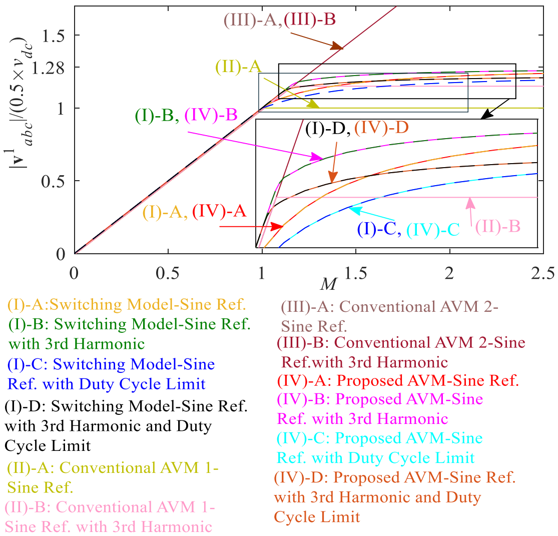

Fig. 5. Output voltage characteristics in the linear and overmodulation regions obtained by the switching model, conventional AVMs, and the proposed AVM.

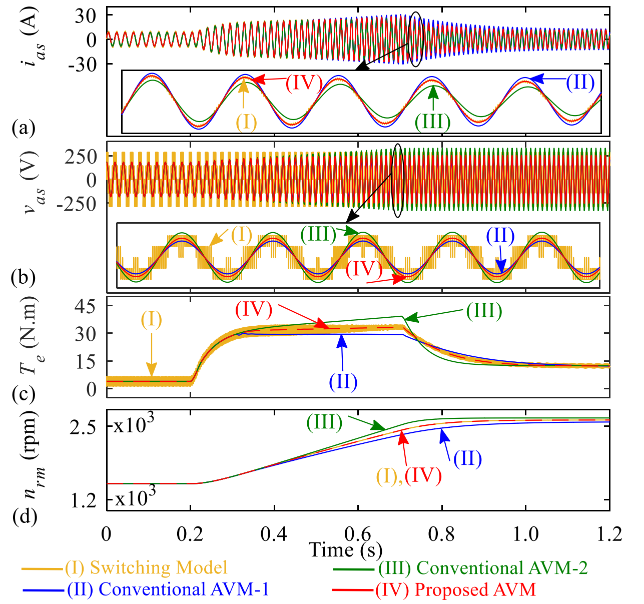

Fig. 6. Transient response during speed command change as predicted by the subject models of VSI with standard SPWM for various motor variables: (a) stator current, (b) stator voltage, (c) torque, and (d) mechanical speed.

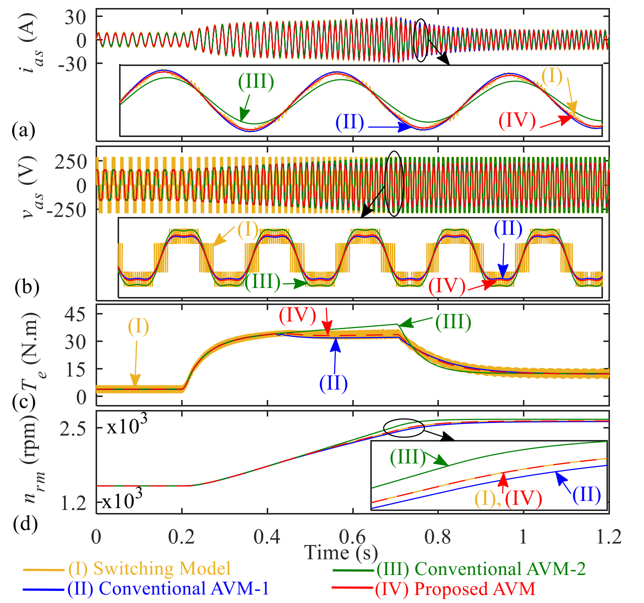

Fig. 7. Transient response during speed command change as predicted by the subject models of VSI with 3rd harmonic injection SPWM for motor variables: (a) stator current, (b) stator voltage, (c) torque, and (d) mechanical speed.

profiles of the conventional AVMs are also shown, with AVM-1 limited to 1 (and 1.15 with 3rd harmonic injection), and linearly increasing unboundedly with AVM-2, as explained in section III–A. Fig. 5 also illustrates how the effective output voltage increases with 3rd harmonic injection and decreases with duty-cycle limit.

IV. Computer Studies

Here, the accuracy of the subject AVMs (i.e., conventional AVM-1 and AVM-2, and the proposed numerical AVM) is investigated in comparison to the detailed switching model under various SPWM schemes for a transient study including speed control. The parameters of the system, including the IM, load, *v/f* controller, slew rate, VSC, and the lookup tables used for the proposed AVM, are summarized in the Appendix.

It is assumed that the motor is initially operating in a steady state with a speed command set at 1500 rpm (corresponding to f_e =50 Hz). At t=0.2 s, the command is stepped up through a slew rate limiter to 2700 rpm (corresponding to f_e =90 Hz), and simulations run until t=1.2 s.

The transient responses of the motor variables, including the stator current i_{as}, stator phase *a* voltage v_{as}, electromagnetic torque T_e, and rotor mechanical speed n_{rm}, are shown in Fig. 6 when purely sinusoidal modulating signals are used in SPWM, and in Fig. 7 when 3rd harmonic injection is used.

Until t=0.2 s with speed command 1500 rpm, VSI operates in the linear modulation region with $M \approx$0.85; and the three AVMs produce identical results that are consistent with the switching model, as seen in Figs. 6, 7. This is also consistent with observations in Fig. 5. However, after t=0.2 s, the speed command of 2700 rpm drives the VSI into the overmodulation region with $M \approx$1.54. As expected, based on Fig. 5 and observed in Figs. 6, 7, the two conventional AVMs fail to capture the correct dynamics in the overmodulation region compared to the switching model. It is observed that AVM-1 exhibits a slower speed response due to underestimating the voltage applied to the motor, because of the imposed modulation limit. Also, AVM-2 predicts an unrealistically fast response due to overestimating the applied voltage/torque, because of the unsaturated output characteristic [see Fig. 5, line (III)-A, B].

In the meantime, the proposed AVM captures the transients in all the motor variables with excellent accuracy compared to the switching model under both switching schemes, as seen in Figs. 6 and 7, that is consistent with observations in Fig. 5.

The 2-norm and maximum error in the speed profile predicted by the three AVMs are calculated and summarized in Tables I and II, for Case-A (i.e., sinusoidal SPWM) and Case-B (i.e., SPWM with 3rd harmonic injection), respectively. As seen in Tables I and II, the errors of the two conventional AVM-1 and AVM-2 can be in the order of ~3–4%; whereas the proposed AVM is almost error-free (~0.01–0.02%).

It is also noted that the reason the two conventional AVMs exhibit less error in Table II (Case-B) compared to Table I

TABLE I. NUMERICAL ACCURACY OF THE SUBJECT AVMS FOR SPEED PROFILE IN CASE-A WITH SINUSOIDAL MODULATING SIGNALS

AVM of VSC	Conventional AVM-1	Conventional AVM-2	Proposed AVM
2-Norm Error	2.03%	2.03%	0.00%
Max Error	3.51%	4.07%	0.01%

TABLE II. NUMERICAL ACCURACY OF THE SUBJECT AVMS FOR SPEED PROFILE IN CASE-B WITH SPWM AND THIRD-HARMONIC INJECTION

AVM of VSC	Conventional AVM-1	Conventional AVM-2	Proposed AVM
2-Norm Error	0.60%	1.40%	0.01%
Max Error	1.15%	3.09%	0.02%

TABLE III. NUMERICAL ACCURACY OF THE PROPOSED AVM FOR SPEED PROFILE IN CASE-C AND CASE-D WITH DUTY-CYCLE LIMIT FOR PWM

Proposed AVM	Case-C	Case-D
2-Norm Error	0.01%	0.01%
Max Error	0.06%	0.02%

(Case-A), is that the linear region is extended with 3rd harmonic injection, where the speed profile has less error compared to the reference solution. Nevertheless, the error in the conventional AVMs may be unacceptable depending on the study objectives.

The 2-norm and maximum error in the profile of the speed predicted by the proposed AVM are also provided in Table III when the duty-cycle limit is considered for the PWM switching schemes, i.e., Case-C with sinusoidal SPWM and Case-D with SPWM and 3rd harmonic injection. Therein, the conventional AVMs are omitted, as they lack the mechanism to incorporate the duty-cycle limit, and the invalidity of their results has already been observed in Figs. 6 and 7 and Tables I and II in the overmodulation region with both standard SPWM and SPWM with 3rd harmonic injection. As shown in Table III, the proposed numerical AVM achieves exceptional accuracy in predicting motor variables, even when the duty-cycle limit is incorporated into the switching scheme. This verifies that the proposed AVM can be a valuable asset for numerically efficient simulations of VSC-driven systems when an accurate representation of both linear and nonlinear characteristics of the converter is desired.

V. CONCLUSION

In this paper, a numerical average-value model (AVM) has been presented for voltage-source converters (VSCs) that can represent their nonlinear characteristics. The proposed AVM was verified under both linear and overmodulation/nonlinear operation using sinusoidal PWM, sinusoidal PWM with 3rd harmonic injection, as well as when the duty-cycle limit is considered for PWM signals in a motor drive system. The proposed AVM uses lookup tables to incorporate (any desired) nonlinearities and was shown to provide an excellent accuracy compared to the detailed switching models of VSCs; and outperformed the existing conventional AVM counterparts that are incapable of capturing the VSC's nonlinear characteristics.

APPENDIX

Parameters of IM [15]: Nominal voltage/power/speed: 220 V/ 3 hp/ 1710 rpm, $P = 4$, $r_s = 0.435\ \Omega$, $r_r' = 0.816\ \Omega$, $x_{ls} = x_{lr}' = 0.754\ \Omega$, $x_m = 26.13\ \Omega$, $J = 0.1157$ kg.m^2.

VSI: $v_{dc} = 430$ V, $f_{sw} = 4$ kHz.

v/f Controller: $\Gamma_{v/f} = 3.67$ V.s, slew rate: ±2390 rpm/s.

Mechanical load: $T_l = k\left(n_{rm}\right)^2$, $k = 1.78\times10^{-6}$.

TABLE IV. LOOKUP TABLE OF THE PROPOSED AVM FOR SPWM

M	0	1	1.1	1.2	1.4	1.6	1.8	2.0	2.2	2.4
M'	0	1	1.065	1.105	1.155	1.185	1.204	1.218	1.228	1.235

TABLE V. LOOKUP TABLE OF THE PROPOSED AVM FOR SPWM WITH 3RD HARMONIC INJECTION

M	0	1	1.1	1.2	1.4	1.6	1.8	2.0	2.2	2.4
M'	0	1	1.10	1.182	1.214	1.230	1.240	1.247	1.252	1.255

TABLE VI. LOOKUP TABLE OF THE PROPOSED AVM FOR SPWM WITH DUTY-CYCLE LIMIT

M	0	1	1.1	1.2	1.4	1.6	1.8	2.0	2.2	2.4
M'	0	1	1.042	1.076	1.119	1.145	1.162	1.174	1.182	1.189

TABLE VII. LOOKUP TABLE OF THE PROPOSED AVM FOR SPWM WITH 3RD HARMONIC INJECTION AND DUTY-CYCLE LIMIT

M	0	1	1.1	1.2	1.4	1.6	1.8	2.0	2.2	2.4
M'	0	1	1.10	1.146	1.171	1.185	1.194	1.20	1.204	1.207

REFERENCES

[1] A. Yazdani and R. Iravani, "A generalized state-space averaged model of the three-level NPC converter for systematic DC-voltage-balancer and current-controller design," *IEEE Trans. Power Del.*, vol. 20, no. 2, pp. 1105–1114, Apr. 2005.

[2] S. Ebrahimi and J. Jatskevich, "Numerically enhanced interfacings for average-value models of voltage-source converters in nodal-based EMT simulators," *Energies*, vol. 18, no. 16, Art. no. 4400, Aug. 2025.

[3] S. Ebrahimi, T. Vahabzadeh, and J. Jatskevich, "Numerically efficient average–value model for voltage-source converters in nodal-based programs," *IEEE Open J. Power Electron.*, vol. 5, pp. 93–105, 2024.

[4] S. Ebrahimi and J. Jatskevich, "Average-value model for voltage-source converters with direct interfacing in EMTP–type solution," *IEEE Trans. Energy Convers.*, vol. 38, no. 3, pp. 2231–2234, Sep. 2023.

[5] S. Ebrahimi, T. Vahabzadeh, and J. Jatskevich, "Direct interfacing of average-value models of VSCs in PSCAD/EMTDC," in *Proc. IEEE Electr. Power Energy Conf. (EPEC)*, BC, Canada, 2022, pp. 452–457.

[6] N. Mohan, T. M. Undeland, and W. P. Robbins, "Power electronics: converters, applications, and design," 2nd ed. New York: John Wiley & Sons, Inc., 1995.

[7] V. Kaura and V. Blasko, "Operation of a voltage source converter at increased utility voltage," *IEEE Trans. Power Electron.*, vol. 12, no. 1, pp. 132–137, Jan. 1997.

[8] Z. Xu, D. Liu, X. Zhao, and J. Ren, "Over–modulation control strategy of SVPWM review," in *Proc. Chinese Control and Decision Conf. (CCDC)*, Yinchuan, China, 2016, pp. 3192–3196.

[9] Jang-Hwan Kim and S. -K. Sul, "Overmodulation strategy for a three-phase four-leg voltage source converter," in *Proc. 38th IAS Ann. Meeting Record Industry App. Conf.*, Salt Lake City, USA, 2003, pp. 656–663.

[10] N. Zhang, Y. Zhou, L. Yang, S. Xu, Z. Zhu and Y. Xiong, "Research on main circuit analysis of VSC-HVDC under over-modulation method," in *Proc. IEEE 4th Int. Conf. on HVDC*, Xi'an, China, 2020, pp. 583–588.

[11] A. M. Hava, R. J. Kerkman and T. A. Lipo, "Carrier–based PWM–VSI overmodulation strategies: analysis, comparison, and design," *IEEE Trans. Power Electron*, vol. 13, no. 4, pp. 674–689, Jul. 1998.

[12] S. Pang, W. Tang, J. Zhang, Y. Zhang, and Z. Yang, "Average model of hybrid modular multilevel converter considering overmodulation," in *Proc. IEEE 26th Int. Conf. Elect. Mach. Syst. (ICEMS)*, Zhuhai, China, 2023, pp. 1729–1734.

[13] Texas Instruments, "UCC28C4x-Q1 automotive BiCMOS low–power current-mode PWM controllers," Datasheet, SLUSA12G, [Online], Available: https://www.ti.com/lit/ds/symlink/ucc28c43-q1.pdf.

[14] A. N. Rahman, H. J. Chiu and K. L. Lian, "Enhanced time average model of three-phase voltage source converter taking dead-time distortion effect into account," *IEEE Access*, vol. 9, pp. 23648–23659, 2021.

[15] P. Krause, O. Wasynczuk, S. Sudhoff, and S. Pekarek, Analysis of Electric Machinery and Drive Systems, Third Edition., vol. 3. Wiley-IEEE Press, 2013.

979-8-3315-8138-1